Low-Temperature Growth and Photoluminescence Property of ZnS Nanoribbons

Zengxing Zhang,[†] Jianxiong Wang,[†] Huajun Yuan,[†] Yan Gao,[†] Dongfang Liu,[†] Li Song,[†] Yanjuan Xiang,[†] Xiaowei Zhao,[†] Lifeng Liu,[†] Shudong Luo,[†] Xinyuan Dou,[†] Shicheng Mou,[‡] Weiya Zhou,[†] and Sishen Xie*[,†]

Institute of Physics, Graduate School of Chinese Academy of Sciences, Chinese Academy of Sciences, Beijing 100080, People's Republic of China, and Nanotechnology Industrialization Base of China, TEDA, Tianjin 300457, People's Republic of China

Received: April 27, 2005; In Final Form: July 18, 2005

At a low temperature of 450 °C, ZnS nanoribbons have been synthesized on Si and KCl substrates by a simple chemical vapor deposition (CVD) method with a two-temperature-zone furnace. Zinc and sulfur powders are used as sources in the different temperature zones. X-ray diffraction (XRD), selected area electron diffraction (SEAD), and transmission electron microscopy (TEM) analysis show that the ZnS nanoribbons are the wurtzite structure, and there are two types—single-crystal and bicrystal nanoribbons. Photoluminescence (PL) spectrum shows that the spectrum mainly includes two parts: a purple emission band centering at about 390 nm and a blue emission band centering at about 445 nm with a weak green shoulder around 510 nm.

Introduction

One-dimensional (1-D) nanoscale semiconductor materials, including nanotubes, nanowires, and nanoribbons (or nanobelts), have been investigated intensively due to their great potential fundamental physical properties and applications in various fields.[1−5] In particular, nanoribbons have attracted lots of attention because they represent an interesting geometrical shape with rectangular cross-section. Zinc sulfide (ZnS), as one of the most important functional materials, exhibits a direct band gap of 3.7 eV at room temperature with a large exciton binding energy of 40 meV.[6,7] It has a high refractive index and is well-known for its photoluminescence[8] and electroluminescence,[9] etc. It is proposed to be applied in various fields, such as flat-panel displays, electroluminescence devices, infrared windows,[10,11] sensors, and lasers.[8,12] These related properties and applications are strongly dependent on structures. Therefore, it is important to control the synthesis of their structures.

Ma et al. have synthesized ZnS nanoribbons without catalysts at 1050 °C.[13] With a method of the hydrogen-assisted thermal evaporation of ZnS powder at the temperature above 1000 °C, Jiang et al. and Yuan et al. have synthesized ZnS nanoribbons, respectively.[14,15] Meng et al. have reported ZnS bicrystal nanoribbons through a process of the thermal evaporation of the mixture of ZnS and SiO at the temperature of 1150 °C.[16] ZnS nanoribbons have been reported by other groups too.[17−22] But all of the above reports reveal that the synthesis of ZnS nanoribbons requires high temperatures. Herein we report a simple chemical vapor deposition (CVD) method with a two-temperature-zone furnace to synthesize ZnS nanoribbons on a large scale at a low temperature of 450 °C with zinc and sulfur powders as sources. Because of the low temperature, the nanoribbons can be synthesized on some low-melting substrates. ZnS nanoribbons have been synthesized on both KCl and Si substrates successfully in our experiment. Transmission electron microscopy (TEM) analysis shows that there are two types—single-crystal and bicrystal nanoribbons. Crystal structural characterization of ZnS nanoribbons with X-ray diffraction (XRD) and selected area electron diffraction (SAED) exhibits that the single-crystal and bicrystal nanoribbons are both wurtzite structure of ZnS.

Experimental Section

ZnS nanoribbons were synthesized with a quartz tube in a two-temperature-zone furnace. Single-crystal KCl and Si wafers were employed as substrates, which were polished at first and then sputter-coated with a thin film of Au as the catalyst. Sulfur powder, KCl (or Si) substrates, and zinc powder were placed in the quartz tube along the gas-flow direction in sequence, and the KCl (or Si) substrates were ∼5 cm away from the zinc powder. The position of the substrates is beneficial for deposition, which is the intercepting spot of the two kinds of vapors (zinc and sulfur) from opposite directions. The zinc powder and the substrates were placed in the temperature zone of 450 °C, and the sulfur powder was placed in the temperature zone of 80 °C. When the process was carried out, the system was maintained at the pressure of 10^{-2} Pa, and argon (Ar; purity, 99.9%; 50 cm^3(STP) min^{-1}) was introduced in as the carrier gas at the same time. After 3 h, the substrates were taken out and cooled rapidly in the protection of Ar. Field emission scanning electron microscopy (FESEM) was employed to analyze the morphology of the products. Energy-dispersive X-ray (EDX), XRD, and TEM were employed to analyze the elemental composition and crystal structure. And the photoluminescence (PL) spectrum was measured with a He−Cd laser with the exciton wavelength of 325 nm.

Results and Discussion

Morphologies. FESEM analysis exhibits that the as-synthesized products have the similar morphologies both on Si and KCl substrates. Representative FESEM images of the as-synthesized products on KCl substrates are shown in Figure 1.

* Corresponding author. Telephone: +86-10-82649081. Fax: +86-10-82640215. E-mail: ssxie@aphy.iphy.ac.cn.
† Chinese Academy of Sciences.
‡ TEDA.

10.1021/jp052199d CCC: $30.25
Published on Web 09/13/2005

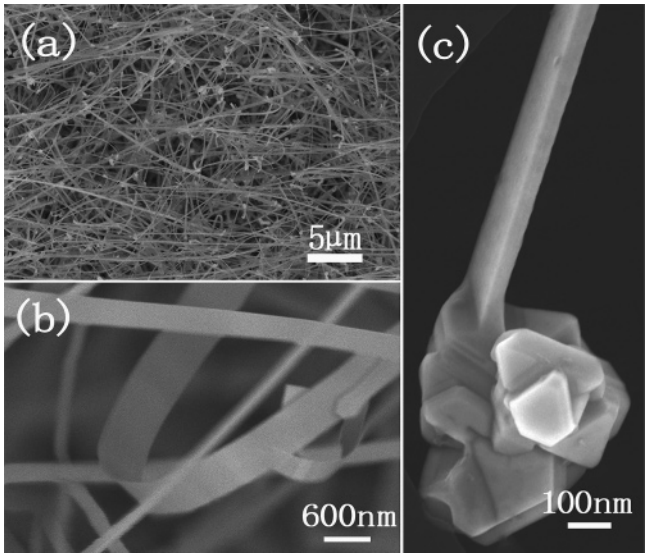

Figure 1. Representative FESEM images of the ZnS nanoribbons: (a) low-magnification FESEM image of the ZnS nanoribbons showing the product in high yield, (b) high-magnification FESEM image, and (c) high-magnification FESEM image of a representative ZnS nanoribbon with many nanocrystals on the bottom.

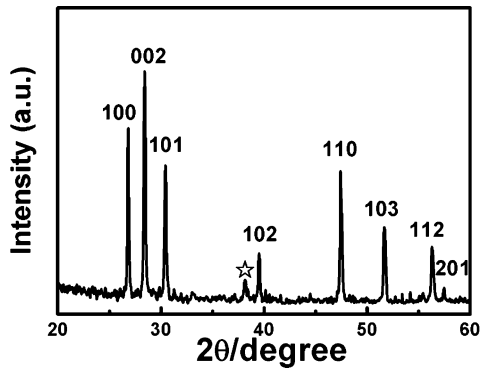

Figure 2. XRD pattern of the as-synthesized ZnS nanoribbons revealing the wurtzite structure. The peak marked with a star corresponds to the Au(111); others correspond to the ZnS wurtzite structure.

The low-magnification FESEM image reveals that the products consist of a large quantity of flexible, various-diameter, and wirelike nanostructures (as shown in Figure 1a). The high-magnification FESEM image shows that they are all nanoribbons from different views (as shown in Figure 1b). The width of the nanoribbons is about several hundreds of nanometers, and the length is about tens of micrometers. The nanoribbons were dissolved from the KCl substrates and transferred to a Cu grid. The observation on FESEM exhibits that there are a few nanocrystals on the bottom of most nanoribbons. The typical FESEM image is shown in Figure 1c.

Structural and Compositional Analysis. The nanoribbons on Si and KCl substrates were both structurally characterized with XRD, exhibiting that they are both the wurtzite structure of ZnS. The typical XRD pattern is shown in Figure 2. Most peaks can be indexed to the wurtzite structure of ZnS with the lattice constants $a = 0.383$ nm and $b = 0.628$ nm, except a peak marked with a star in the XRD pattern, which is according to the (100) plane of Au employed as the catalyst in the experiment.

The structure and morphologies of the ZnS nanoribbons were further characterized with TEM and EDX. Figure 3a is a typical TEM image, which shows that each nanoribbon has uniform width and thickness along the entire length and there are two

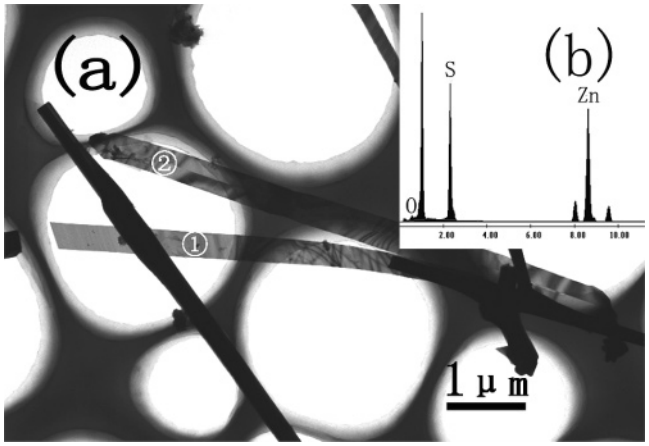

Figure 3. TEM and EDX spectra. (a) TEM image showing that there are two types of ZnS nanoribbons: (①— single-crystal and (②— bicrystal. (b) EDX spectrum of the ZnS nanoribbons.

types—single-crystal and bicrystal nanoribbons—in the as-synthesized products. In Figure 3a, the nanoribbon marked ① is single-crystal with the smooth surface, but ② is bicrystal with a clear boundary at the center of the nanoribbon. Detailed investigation exhibits that the bicrystal nanoribbons are about 30% in the products. Figure 3b is the in-situ EDX spectrum of the nanoribbons. Elemental analysis reveals that the atomic percentages of S and Zn are 46.9 and 46.4%, respectively, and the rest is O. Perhaps the O is due to two reasons—the oxygen absorbed on the surface and that EDX is not sensitive to light elements. Considering the result of XRD and that the ratio of S and Zn is nearly 1:1 in atomicity, it can be concluded that there are very few other materials in the as-synthesized products.

High-resolution TEM (HRTEM) and SAED were employed to analyze the two types of nanoribbons. Investigations of HRTEM and SAED exhibit that there are two types of growth modes for the single-crystal nanoribbons. Figure 4a is a typical HRTEM image of the first type of the single-crystal nanoribbons, and the inset is the corresponding SAED pattern. The SAED pattern can only be indexed as the ZnS wurtzite structure with the incident electron beam parallel to the [001] orientation. As shown in the HRTEM image, the lattice spacing is about 0.328 nm, which corresponds to the spacing for the (010) planes of the ZnS wurtzite structure. Further investigation indicates that the growth direction is along with the [2−10] orientation and the {001} planes are taken as the side surfaces.

Figure 4b shows the HRTEM image of the second type of the single-crystal nanoribbons. The SAED pattern with the incident electron beam parallel to the $[2\bar{1}0]$ orientation indicates that it is the ZnS wurtzite structure (as shown in the inset of Figure 4b). The lattice spacing is 0.630 nm, which corresponds to the spacing for the (001) planes. The growth direction is [001] and this type of single-crystal nanoribbons takes $\{2\bar{1}0\}$ as the side surfaces. Further investigation exhibits that the ratio of the above two single-crystal nanoribbons is about 2:1 in sequence.

The HRTEM image and the corresponding SAED pattern of the bicrystal nanoribbons are shown in Figure 5, where the incident electron beam is parallel to the $[2\bar{1}0]$ direction of the ZnS wurtzite structure. In the HRTEM image of Figure 5a, there is a clear boundary parallel to the [103] direction, which is a symmetric tilt boundary and the growth direction. The angle of the two (001) planes belonging to the different areas is about 64.4°. The corresponding SAED pattern includes two sets of spots (as shown in Figure 5b). Each set of spots corresponds to the ZnS wurtzite structure with a $[2\bar{1}0]$ zone axis.

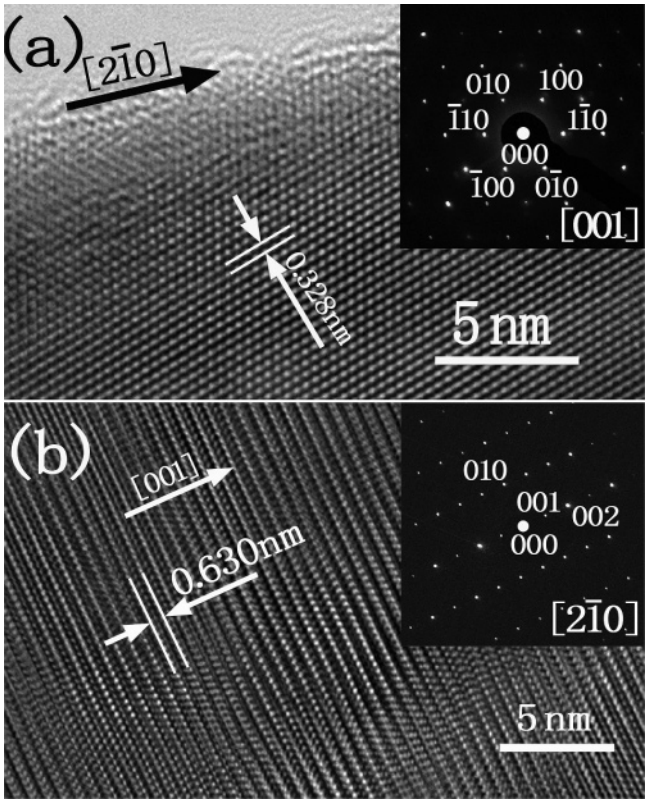

Figure 4. HRTEM images and SAED patterns of single-crystal nanoribbons. (a) The nanoribbon taking {001} planes as side surfaces and its SAED pattern in the corresponding inset. The arrow indicates the corresponding growth direction. (b) The nanoribbon taking {2$\bar{1}$0} planes as side surfaces and its SAED pattern in the corresponding inset. The arrow indicates the corresponding growth direction.

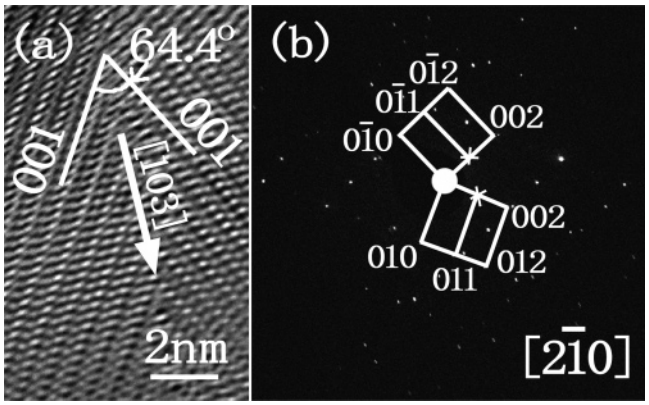

Figure 5. (a) HRTEM image and (b) corresponding SAED pattern of the ZnS bicrystal nanoribbon. The arrow in a indicates the borderline and growth direction.

Growth Mechanism. A detailed investigation of the growth mechanism of the ZnS nanoribbons is currently in process. It has been mentioned above that many ZnS nanocrystals can be observed on the bottom of most nanoribbons, while they are dissolved from the KCl substrate (Figure 1c). It seems that the growth process includes two steps. First, ZnS crystals grow on the substrates. Zinc vapor diffuses and meets the sulfur vapor coming from the opposite direction. They grow into ZnS crystals with the help of Au and disperse on the substrates randomly.

$$\mathrm{Zn(g) + S(g) \rightarrow ZnS(s)}$$

Second, nanoribbons grow from these crystals. The crystals just play the role of seeds and facilitate the growth of ZnS nanoribbons. Generally, the [001] direction is the favorite growth direction of the wurtzite ZnS nanoribbons. But in our experiments, most of them grow along the [2$\bar{1}$0] direction (the ratio of [2$\bar{1}$0] and [001], 2:1). Perhaps that is due to the low temperature of the growth. Meng et al. have analyzed the growth mechanism of ZnS bicrystal nanoribbons.[16] They believed that Si played an important role in the process of the growth. Such a role is not introduced in our experiments. The growth mechanism of bicrystal nanoribbons needs further investigations.

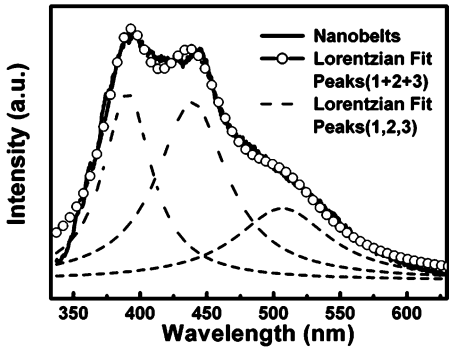

Figure 6. PL spectrum of the ZnS nanoribbons.

Photoluminescence Property. The PL measurement of the ZnS nanoribbons was carried out at room temperature with a He−Cd laser. The exciton wavelength is 325 nm. The PL spectra on different substrates show almost an identical nature. As shown in Figure 6, a typical spectrum mainly includes two parts: a purple emission band centering at about 390 nm and a blue emission band centering at about 445 nm with a weak green shoulder around 510 nm. A multipeak Lorentzian fit gives three Lorentzian bands centering at 390, 439, and 507 nm, respectively. As shown in Figure 6, the Lorentzian curve fits well with the experimental curve. Therefore, the PL spectrum mainly consists of three emission bands at 390, 439, and 507 nm. The emission bands centered at about 390 and 439 nm should be assigned to the stoichiometric vacancies or interstitial impurities in the ZnS nanoribbons, which has been reported by some literature.[21−24] Xu et al. have observed a green emission band centered at 507 nm in Cu-doped ZnS nanocrystals.[25] In some literature, the emission band around 510 nm was proposed to be due to Au impurities.[24,26] In our experiment, Au has been employed as the catalyst. The emission band around 510 nm should be due to Au impurities.

Conclusions

In summary, at the low temperature of 450 °C, ZnS nanoribbons have been synthesized on KCl and Si substrates by a simple CVD method with a two-temperature-zone furnace. Zinc and sulfur powders are used as sources in the different temperature zones. The nanoribbons are the wurtzite crystal structure, and there are two types—single-crystal and bicrystal nanoribbons. The PL spectrum shows that the spectrum mainly includes two parts: the purple emission band centered at about 390 nm and the blue emission band centered at about 445 nm with the weak green shoulder around 510 nm.

Acknowledgment. We would like to express our sincere gratitude to Prof. Gang Wang, Prof. Lianfeng Sun, Prof. Peng Jiang, Prof. Xiaochun Wu, and Dr. Jianjun Zhou for their useful discussions and Prof. Chaoying Wang for FESEM images. The work was supported by the National Natural Science Foundation of China and the "973" National Key Basic Research Item.

References and Notes

(1) Wu, J. J.; Liu, S. C.; Wu, C. T.; Chen, K. H.; Chen, L. C. *Appl. Phys. Lett.* **2002**, *81*, 1312.

(2) Huang, M. H.; Mao, S.; Feick, H. N.; Yan, H. Q.; Wu, Y. Y.; Kind, H.; Weber, E.; Russo, R.; Yang, P. D. *Science* **2001**, *292*, 897.

(3) Holmes, J.; Johnston, K.; Doty, D.; Korgel, B. *Science* **2000**, *287*, 1471.

(4) Hu, J.; Odom, T.; Lieber, C. *Acc. Chem. Res.* **1999**, *32*, 435.

(5) Pan, Z. W.; Dai, Z. R.; Wang, Z. L *Science* **2001**, *291*, 1947.

(6) Menner, R.; Dimmler, B.; Mauch, R.; Schock, H. *J. Cryst. Growth* **1988**, *86*, 906.

(7) Trindade, T. *Chem. Mater.* **2001**, *13*, 3843.

(8) Falcony, C.; Garcia, M.; Ortiz, A.; Alonso, J. C. *J. Appl. Phys.* **1992**, *72*, 1525.

(9) Tang, W.; Cameron, D. C. *Thin Solid Films* **1996**, *280*, 221.

(10) Bredol, M.; Merichi, J. *J. Mater. Sci.* **1998**, *33*, 471.

(11) Calandra, P.; Goffredi, M.; Liveri, V. T. *Colloids Surf., A* **1999**, *160*, 9.

(12) Prevenslik, T. V. *J. Lumin.* **2000**, *87*−*89*, 1210.

(13) Ma, C.; Moore, D.; Li, J.; Wang, Z. L. *Adv. Mater.* **2003**, *15*, 228.

(14) Jiang, Y.; Meng, X. M.; Liu, J.; Xie, Z. Y.; Lee, C. S.; Lee, S. T. *Adv. Mater.* **2003**, *15*, 323.

(15) Yuan, H. J.; Xie, S. S.; Liu, D. F.; Yan, X. Q.; Zhou, Z. P.; Ci, L. J.; Wang, J. X.; Gao, Y.; Song, L.; Liu, L. F.; Zhou, W. Y.; Wang, G. *J. Cryst. Growth* **2003**, *258*, 225.

(16) Meng, X. M.; Jiang, Y.; Liu, J.; Lee, C. S.; Bello, I.; Lee, S. T. *Appl. Phys. Lett.* **2003**, *83*, 2244.

(17) Zhu, Y. C.; Bando, Y.; Xue, D. F. *Appl. Phys. Lett.* **2003**, *82*, 1769.

(18) Li, Q.; Wang, C. *Appl. Phys. Lett.* **2003**, *83*, 359.

(19) Ding, Y.; Wang, X. D.; Wang, Z. L. *Chem. Phys. Lett.* **2004**, *398*, 32.

(20) Gong, J. F.; Yang, S. G.; Duan, J. H.; Zhang, R.; Du, Y. W. *Chem. Commun.* **2005**, *3*, 351.

(21) Kar, S.; Chaudhuri, S. *J. Phys. Chem. B* **2005**, *109*, 3298.

(22) Hu, P. A.; Liu, Y. Q.; Fu, L.; Cao, L. C.; Zhu, D. B. *J. Phys. Chem. B* **2004**, *108*, 936.

(23) Denzler, D.; Olschewski, M.; Sattler, K. *J. Appl. Lett.* **1998**, *84*, 2841.

(24) Xiong, Q. H.; Chen, G.; Acord, J. D.; Liu, X.; Zengel, J. J.; Gutierrez, H. R.; Redwing, J. M.; Lew Yan Voon, L. C.; Lassen, B.; Eklund, P. C. *Nano Lett.* **2004**, *4*, 1663.

(25) Xu, S. J.; Chua, S. J.; Liu, B.; Gan, L. M.; Chew, C. H.; Xu, G. Q. *Appl. Phys. Lett.* **1998**, *73*, 478.

(26) Wang, Y. W.; Zhang, L. D.; Liang, C. H.; Wang, G. Z.; Peng, X. S. *Chem. Phys. Lett.* **2002**, *357* (3−4), 314.